

# First Principles Phase Diagram Calculations for the System NaNbO<sub>3</sub>-KNbO<sub>3</sub>: can spinodal decomposition generate relaxor ferroelectricity?

B.P. Burton\*

*Materials Science and Engineering Laboratory,  
Ceramics Division National Institute of Standards and  
Technology (NIST), Gaithersburg, MD 20899, USA<sup>†</sup>*

Takeshi Nishimatsu

*Institute for Materials Research (IMR),  
Tohoku University, Sendai 980-8577, Japan.*

(Dated: August 8, 2007)

## Abstract

First principles based phase diagram calculations were performed for the system (1-X)·NaNbO<sub>3</sub>-(X)·KNbO<sub>3</sub>. Planewave pseudopotential calculations of formation energies were used as a basis for fitting a cluster expansion Hamiltonian, and a phase diagram was calculated. The predicted phase diagram has an unusually asymmetric miscibility gap that suggests it might be possible to synthesize a lead-free compositionally modulated sample with bulk composition  $X \approx 0.23$ ; such a sample is likely to exhibit relaxor characteristics.

Key words: NaNbO<sub>3</sub>-KNbO<sub>3</sub>; First Principles; Phase diagram calculation; lead-free; relaxor ferroelectric; spinodal decomposition.

Submitted to **Applied Physics Letters** 04/04/2007, Resubmitted 07/03/2007, Accepted 08/06/2007

Typically, when  $\text{Na}^+$  and  $\text{K}^+$  mix on the same crystallographic site of a solid solution the system exhibits a miscibility gap: e.g.  $\text{NaCl-KCl}$ <sup>1,2</sup>;  $\text{NaAlSi}_3\text{O}_8\text{-KAlSi}_3\text{O}_8$ <sup>3</sup>;  $\text{NaNO}_3\text{-KNO}_3$ <sup>4</sup>;  $\text{Na}_3\text{K(AlSiO}_4)_4\text{-K}_4(\text{AlSiO}_4)_4$ <sup>5</sup>. Hence it seems likely that  $(1-X)\cdot\text{NaNbO}_3\text{-(X)}\cdot\text{KNbO}_3$  will also exhibit low temperature (T) immiscibility, even though it was not reported in previous studies<sup>7,8</sup>. Ahtee and Hewat<sup>8</sup> studied phase transitions below 923K in samples that were sintered at 1323 K for 200 h, thus without slow cooling or long-term annealing, low-T immiscibility might well have escaped detection. Also, in the analogous system  $(1-X)\cdot\text{NaTaO}_3\text{-(X)}\cdot\text{KTaO}_3$ , Davis<sup>6</sup> reports possible immiscibility in the composition range  $0.16 \leq X \leq 0.26$ .

Recently there has been great interest in Pb-free piezoelectrics to replace  $\text{Pb(Zr}_{1-X}\text{,Ti}_X\text{)O}_3$ , which is the most widely used transducer, actuator and ferroelectric-sensor material; e.g.<sup>9-11</sup>. Also, because of their desirable dielectric properties, there has been great interest in Pb-free relaxor ferroelectrics (relaxors), e.g.<sup>12-15</sup>. As discussed by several authors, e.g.<sup>16-19</sup>, relaxor characteristics arise because of local "random" fields that are caused by chemical disorder of differently charged- or sized-ions, or by polar defects. In  $\text{NaNbO}_3\text{-KNbO}_3$ , the different ionic sizes of  $\text{Na}^+$  and  $\text{K}^+$  would presumably give rise to strain mediated random fields, but the spatial average strength of these fields,  $\langle h_i \rangle$  is evidently small, or conventionally prepared  $(1-X)\cdot\text{NaNbO}_3\text{-(X)}\cdot\text{KNbO}_3$  samples should exhibit relaxor properties. Immiscibility of Na- and K-rich solid solutions might, however, permit sufficient enhancement of  $\langle h_i \rangle$  to induce relaxor properties; via compositional fluctuations (chemical clustering) that arise from spinodal decomposition<sup>20</sup>. An apparent example of relaxor-enhancement via chemical clustering is  $\text{Ba(Ti}_{1-X}\text{,Zr}_X\text{)O}_3$  in which X-ray absorption fine structure studies<sup>15</sup> indicate significant Zr-clustering in samples with  $0.25 \leq X \leq 0.35$ .

Formation energies,  $\Delta E_f$  (Fig. 1) were calculated for fully relaxed  $\text{NaNbO}_3$  (20 atom cell),  $\text{KNbO}_3$  (5 atom cell), and 49  $\text{Na}_m\text{K}_n\text{Nb}_{(m+n)}\text{O}_{3(m+n)}$  supercells. All calculations were performed with the Vienna *ab initio* simulation program (VASP, version 445<sup>21,22</sup>) using ultrasoft Vanderbilt type plane-wave pseudopotentials<sup>23</sup> with the generalized gradient approximation for exchange and correlation energies. Electronic degrees of freedom were optimized with a conjugate gradient algorithm, and both cell constant and ionic positions were fully relaxed. Pseudopotential valence electron configurations were: Na\_pv  $2p^63s^1$ ; K\_pv  $3p^64s^1$ ; Nb\_pv  $5s^14d^4$ ; O\_s  $3s^23p^4$ .

Total energy calculations were converged with respect to k-point meshes by using the

equivalent of 6 6 6, or greater, for a five-atom  $\text{Pm}\bar{3}\text{m}$  perovskite cell. A 500 eV energy cutoff was used, in the "high precision" option which guarantees that *absolute* energies are converged to within a few meV/mol (a few tenths of a kJ/mol of exchangeable cations;  $\text{Na}^+$  or  $\text{K}^+$ ; one mol =  $\text{Na}_{1-X}\text{K}_X\text{NbO}_3$ ). Residual forces were typically of the order of 0.02 eV or less. To obtain fully relaxed structures, it was *not* sufficient to perform conventional relaxations without symmetry constraints. Rather, T-dependent molecular dynamics (MD) annealing, typically at 300 K, followed by normal 0 K relaxations lead to significant reductions in calculated values for  $\Delta E_f$ . Performing additional annealing steps, however, never yielded significant additional reductions in  $\Delta E_f$ . Figure 1 exhibits the results of conventional 0 K relaxations ( $\circ$ ); and the 0 K relaxations that followed MD-annealing ( $\square$ ); dotted lines are to guide the eye.

Calculated formation energies,  $\Delta E_f$ , for 49  $\text{Na}_m\text{K}_n\text{Nb}_{(m+n)}\text{O}_{3(m+n)}$  supercells are plotted in Fig. 1, where values for  $\Delta E_f$  are normalized per mol of exchangeable  $\text{Na}^+$  and  $\text{K}^+$  ions:

$$\Delta E_f = (E_S - mE_{\text{NaNbO}_3} - nE_{\text{KNbO}_3})/(m+n) \quad (1)$$

Here:  $E_S$  is the total energy of the  $\text{Na}_m\text{K}_n\text{Nb}_{(m+n)}\text{O}_{3(m+n)}$  supercell;  $E_{\text{NaNbO}_3}$  is the energy/mol of  $\text{NaNbO}_3$ ;  $E_{\text{KNbO}_3}$  is the energy/mol of  $\text{KNbO}_3$ .

All supercell energies are positive which indicates a miscibility gap system.

The cluster expansion,  $\text{CE}^{24}$ , is a compact representation of the configurational total energy. In the  $(1-X)\cdot\text{NaNbO}_3\text{-}(X)\cdot\text{KNbO}_3$  quasibinary system, the solid solution configuration is described by pseudospin occupation variables  $\sigma_i$ , which take values  $\sigma_i = -1$  when site- $i$  is occupied by  $\text{Na}^+$  and  $\sigma_i = +1$  when site- $i$  is occupied by  $\text{K}^+$ .

The CE parameterizes the configurational energy, per exchangeable cation, as a polynomial in pseudospin occupation variables:

$$E(\sigma) = \sum_{\ell} m_{\ell} J_{\ell} \left\langle \prod_{i \in \ell'} \sigma_i \right\rangle \quad (2)$$

Cluster  $\ell$  is defined as a set of lattice sites. The sum is taken over all clusters  $\ell$  that are not symmetrically equivalent in the high-T structure space group, and the average is taken over all clusters  $\ell'$  that are symmetrically equivalent to  $\ell$ . Coefficients  $J_{\ell}$  are called effective cluster interactions, ECI, and the *multiplicity* of a cluster,  $m_{\ell}$ , is the number of symmetrically

equivalent clusters, divided by the number of cation sites. The ECI are obtained by fitting a set of VASP FP calculated structure energies,  $\{E_{Str}\}$ . The resulting CE can be improved as necessary by increasing the number of clusters  $\ell$  and/or the number of  $E_{Str}$  used in the fit.

Fitting was performed with the Alloy Theoretic Automated Toolkit (ATAT)<sup>22,25–27</sup> which automates most of the tasks associated with the construction of a CE Hamiltonian. A complete description of the algorithms underlying the code can be found in<sup>26</sup>. The most important steps are: 1) Selecting which first principles (FP) structure energies to calculate, which is done in a way that minimizes the statistical variance of the estimated ECI; 2) Automatically selecting which clusters to include in the expansion by minimizing the *cross-validation score*,  $CV$ :

$$(CV)^2 = \frac{1}{N} \sum_{Str=1}^N (E_{Str} - \hat{E}_{Str})^2 \quad (3)$$

where  $E_1, \dots, E_N$  denote the structural energies calculated from FP and  $\hat{E}_{Str}$  is the energy of structure  $Str$  predicted from a CE that was fit to the remaining  $N - 1$  energies. This criterion ensures that the chosen set of clusters maximizes the predictive power of the CE for any structure, whether or not it is included in the fit. This is an improvement relative to the standard mean square error criterion which only minimizes the error for structures that are included in the fit. The optimized cluster set, Table I, includes 12 pairs, six triplets and three 4-body terms;  $CV^2 = 0.011$  eV. The ECI were fit to all 49 of the  $E_{Str}$  plotted on Fig. 1 ( $\square$ ), in which filled diamonds ( $\blacklozenge$ ) indicate  $\Delta E_f$  that were calculated with the CE and the solid curve (green on line) is the high-T CE-expansion limit of the total energy. The  $\sim 1$  kJ/mol overestimate of  $E_{NaNbO_3}$  suggests a small, of order 10%, underestimation of the consolute temperature,  $T_C$ .

In addition to the CV-criterion, ATAT also ensures that ground states predicted from the CE agree with the minimum energy structures for each composition, as calculated from FP. The code proceeds by iterative refinement, gradually increasing the number of clusters and the number of structures to provide the best possible fit based on the current set  $\{E_{Str}\}$ .

First principles phase diagram (FPPD) calculations were performed with canonical Monte Carlo (MC) simulations using the emc2 code which is part of the ATAT package<sup>25–27</sup>. Input parameters for emc2 were: a 29x29x29 unit cell simulation box; 1500 equilibration passes;

1500 Monte Carlo passes. The predicted phase diagram is shown in Figure 2, in which, open circles indicate equilibrated MC simulations. The predicted consolute point is approximately  $\{X_C, T_C\} \sim \{0.23, 1720 \text{ K}\}$ . The dramatic asymmetry of this diagram strongly suggests short-range Na:K order based on a bulk composition near 1:1 at  $T \geq 550 \text{ K}$ , but attempts to identify a stable phase in this region of the  $\{X, T\}$  space were unsuccessful.

Typically, FPPD calculations overestimate consolute temperatures especially when, as here, the excess vibrational contribution to the free energy is ignored. Including this contribution, however, usually leads to only a 5-15% reduction in  $T_C$ <sup>28</sup>, which would not alter the conclusions of this work. The predicted miscibility gap on the Na-rich side of the  $\text{NaNbO}_3 - \text{KNbO}_3$  phase diagram suggests the possibility of synthesizing relaxor ferroelectrics by slowly cooling a sample with a bulk composition near  $\text{Na}_{0.77}\text{K}_{0.23}\text{NbO}_3$ . Spinodal decomposition induced Na:K concentration waves is expected to concentrate local fields in a way that promotes and enhances relaxor properties. Simulations of  $\text{Pb}(\text{Mg}_{1/3}\text{Nb}_{2/3})\text{O}_3$  and  $\text{Pb}(\text{Sc}_{1/2}\text{Nb}_{1/2})\text{O}_3$ <sup>18,19</sup> indicate that chemical short-range order enhances relaxor properties, relative to a system with random chemical disorder. Similarly, X-ray absorption fine structure studies of  $\text{Ba}(\text{Ti}_{1-X}\text{Zr})_X\text{O}_3$  ( $0.25 \leq X \leq 0.35$ )<sup>15</sup> correlate chemical clustering of Zr with enhanced relaxor properties. Thus, it is reasonable to expect a similar effect from spinodal decomposition induced Na:K clustering in  $\text{NaNbO}_3 - \text{KNbO}_3$ .

## ACKNOWLEDGEMENT

Most of the total energy calculations for this work were performed by B.P. Burton, in the Kawazoe Laboratory of the Institute for Materials Research (IMR), Tohoku University, Sendai 980-8577, Japan while he was there as a visiting professor in 2005.

- 
- \* Electronic address: `benjamin.burton@nist.gov`
- † Phone: 301-975-6053, FAX: 301-975-5334.
- <sup>1</sup> Thompson, J.B. and Waldbaum, D.R. (1969). *Geochimica et Cosmochimica Acta*, **33**, 671-690.
- <sup>2</sup> B.P. Burton and A. van de Walle, *Chemical Geology*, **225** 222-229, (2006).
- <sup>3</sup> R. A. Yund and J. Tullis, "Feldspar Mineralogy," *Reviews in Mineralogy*, V2, Chapter 6, 141-  
Mineralogical Society of America, P. H. Ribbe Ed. (1983).
- <sup>4</sup> E. M. Levin, C. R. Robins and H. F. McMurdie, "Phase Diagrams for Ceramists" diagram 1047,  
American Ceramic Society, (1964).
- <sup>5</sup> J. M. Ferry and J. G. Blencoe, *Am. Mineral.* **63** 1225 (1978).
- <sup>6</sup> T. G. Davis, *Phys. Rev. B* **5** 2530 (1972).
- <sup>7</sup> G. Shirane, R. Newnham and R. Pepinsky, *Phys. Rev.* **96**[3] 581 (1954).
- <sup>8</sup> M. Ahtee and A. W. Hewat, *Acta Cryst. A* **34** 309 (1978).
- <sup>9</sup> P. Baettig, C. F. Schelle, R. LeSar, U. V. Waghmare and N. Spaldin, *Chem. Mater* **17** 1376  
(2005).
- <sup>10</sup> R. E. Eitel, C. A. Randall, T. R. Shrout, P. W. Rehrig, W. Hackenberger and S.-E. Park *Jpn.*  
*J. Appl. Phys.* **40** 5999 (2001).
- <sup>11</sup> J. Iniguez, D. Vanderbilt, L. Belliache, *Phys. Rev. B* **67** 224107 (2003).
- <sup>12</sup> A. Simon, J. Ravez and M. Maglione, *J. Phys. Condens. Matter* **16** 963 (2004).
- <sup>13</sup> V. A. Shuvaeva, D. Zekria, A. M. glazer, Q. Jiang, S. M. Weber, P. Bhattacharya and P. A.  
Thomas, *Phys. Rev. B* **71** 174114 (2005).
- <sup>14</sup> V. Bobnar, B. Malič, J. Holc, M. Kosec, R. Steinhausen and H. Beige, *J. Appl Phys.* **98** 024113  
(2005).
- <sup>15</sup> C. Laulhé, F. Hippert, J. Kreisel, M. Maglione, A. Simon, J. L. Hazemann and V. Nassif, *Phys.*  
*Rev. B* **74** 014106 (2006).
- <sup>16</sup> H. Quian and L.A. Bursill, *Int. J. Mod. Phys.* **10**, 2027 (1996).
- <sup>17</sup> W. Kleemann, G. A. Samara and J. Dec, "Polar Oxides: Properties, Characterization, and  
Imaging" R. Waser, U. Bottger and S. Tiedke Editors, WILEY-VCH Verlag GmbH & Co.  
KGaA, Weinheim P.P. 275 (2005) ISBN: 3-527-40532-1.
- <sup>18</sup> B.P. Burton, E. Cockayne, S. Tinte, and U.V. Waghmare, *Phase Transitions* **79**, 91 (2006).

- <sup>19</sup> S. Tinte, B.P. Burton, E. Cockayne, and U. V. Waghmare, Phys. Rev. Lett. **97**, 137601 (2006).
- <sup>20</sup> J.W. Cahn, Acta Metall. **9** 795 (1961).
- <sup>21</sup> Kresse, G. and Hafner, J., Phys. Rev. **B47**: 558-561 (1993); Kresse, G. Thesis, Technische Universität Wien (1993); Phys. Rev. **B49**: 14 251 (1994). Kresse, G. and Furthmüller, J. (1996) Comput. Mat. Sci. **6**: 15-50; Phys. Rev. **B54**: 11169 (1996); cf. <http://tph.tuwien.ac.at/vasp/guide/vasp.html>.
- <sup>22</sup> Reference to specific software packages does not imply a NIST endorsement.
- <sup>23</sup> Vanderbilt, D. Phys. Rev. **B41**: 7892 (1990).
- <sup>24</sup> Sanchez, J.M., Ducastelle, F. and Gratias, D., (1984). Physica **128A**, 334-350.
- <sup>25</sup> van de Walle, A., Asta, M. and Ceder, G. The alloy theoretic automated toolkit: A user guide. CALPHAD Journal **26** p. 539 (2002).
- <sup>26</sup> van de Walle A. and Ceder, G., Journal of Phase Equilibria, **23** p. 348 (2002).
- <sup>27</sup> van de Walle, A. and Asta, M. Self-driven lattice-model monte carlo simulations of alloy thermodynamic properties and phase diagrams. Modelling Simul. Mater. Sci. Eng., **10** p. 521 (2002).
- <sup>28</sup> van de Walle A. and Ceder, G., Rev. Mod. Phys. **74**, 11 (2002).

TABLE I: Effective Cluster Interactions in  $eV/mol$ .

Cluster Coordinates	$m_\ell$	ECI: $J_\ell$
minus (1,1,1)	Multiplicity	eV/cation
Zero Cluster	1	0.048604
Point Cluster	1	-0.036733
(1,0,1)	3	0.002674
(0,2,1)	6	0.002150
(0,0,0)	4	-0.000911
(1,1,-1)	3	-0.003070
(1,0,-1)	12	0.000694
(2,2,3)	12	0.000012
(-1,3,1)	6	-0.000473
(1,1,-2)	3	-0.001115
(0,-1,-1)	12	-0.001186
(1,0,-2)	12	-0.001124
(0,0,-2)	12	-0.000485
(-1,-1,-1)	4	0.000789
(0,1,1), (0,2,1)	12	-0.000311
(0,1,2), (0,2,1)	8	-0.000450
(1,0,0), (0,0,0)	24	0.000628
(1,1,0), (1,1,-1)	3	0.000961
(1,0,0), (1,1,-1)	12	0.001368
(0,0,0), (1,1,-1)	12	0.000235
(1,2,2), (0,1,2), (0,2,1)	2	0.003103
(0,1,0), (1,0,0), (0,0,0)	24	-0.000773
(0,1,0), (1,0,0), (1,1,-1)	12	-0.001022



## FIGURE CAPTIONS

Figure 1) Comparison of VASP formation energies,  $\Delta E_f$ , that were calculated by conventional 0 K relaxations ( $\circ$ , “No MD”) with  $\Delta E_f$  from 0 K relaxations that followed 300 K annealing runs ( $\square$ , “MD”). Filled diamonds ( $\blacklozenge$ ) indicate the cluster-expansion fit to the annealed set, and the solid curve is the high temperature cluster expansion limit for the total energy.

Figure 2) Calculated phase diagram, based on the cluster expansion that was fit to the annealed set of formation energies ( $\square$ , “MD” in Fig. 1). Note the unusually asymmetric miscibility gap.

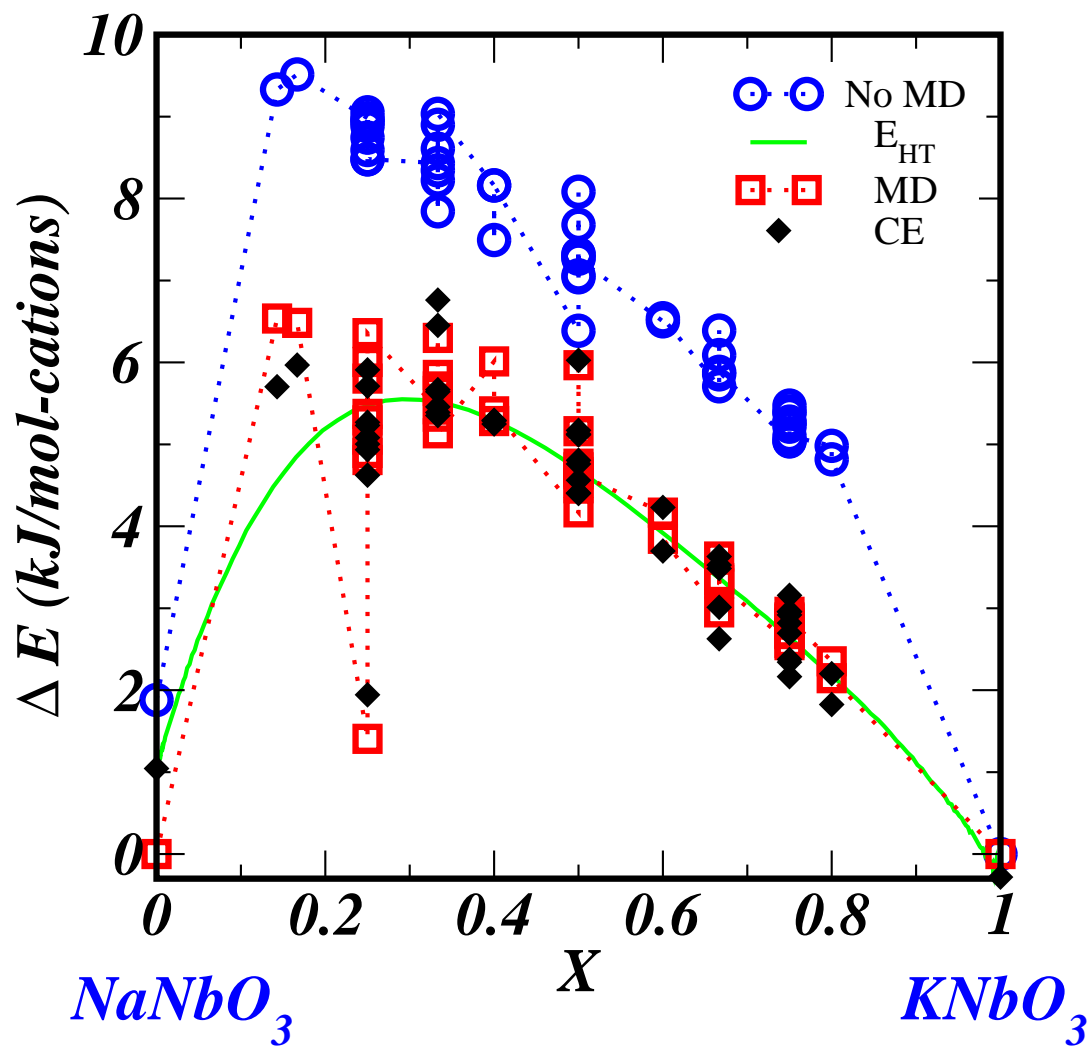


FIG. 1: Comparison of VASP formation energies,  $\Delta E_f$ , that were calculated by conventional 0 K relaxations ( $\circ$ , “No MD”) with  $\Delta E_f$  from 0 K relaxations that followed 300 K annealing runs ( $\square$ , “MD”). Filled diamonds ( $\blacklozenge$ ) indicate the cluster-expansion fit to the annealed set, and the solid curve is the high temperature cluster expansion limit for the total energy.

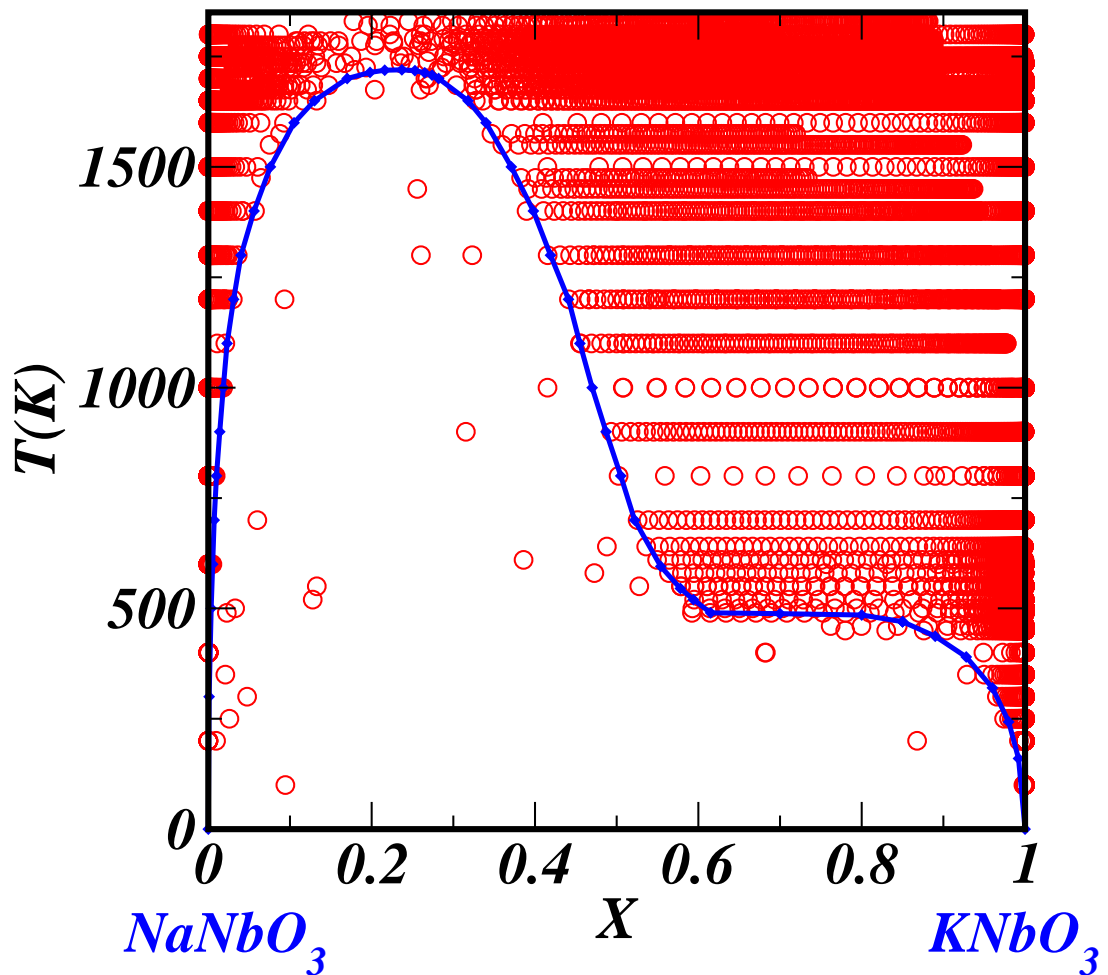


FIG. 2: Calculated phase diagram, based on the cluster expansion that was fit to the annealed set of formation energies ( $\square$ , “MD” in Fig. 1”). Note the unusually asymmetric miscibility gap.